ACCOUNTS
of chemical research

Chemistry at the Dirac Point: Diels–Alder Reactivity of Graphene

SANTANU SARKAR, ELENA BEKYAROVA, AND
ROBERT C. HADDON*

Center for Nanoscale Science and Engineering, Departments of Chemistry and Chemical & Environmental Engineering, University of California, Riverside, California 92521-0403, United States

RECEIVED ON NOVEMBER 23, 2011

CONSPECTUS

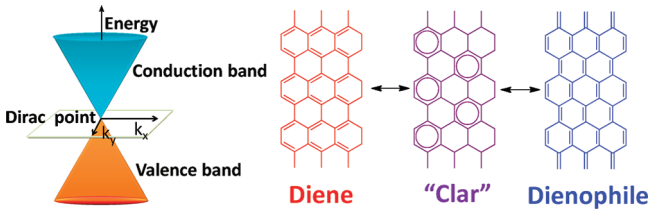

Most of the interesting physics of graphene results from the singular electronic band structure at the so-called Dirac point, where the conduction and valence bands cross in momentum space. Although graphene is very stable thermodynamically, the electronic structure at the Dirac point facilitates basal plane chemistry including pericyclic reactions such as the Diels–Alder reaction.

We have discovered a series of facile Diels–Alder reactions in which graphene can function either as a diene when paired with tetracyanoethylene and maleic anhydride or as a dienophile when paired with 2,3-dimethoxybutadiene and 9-methylanthracene. In this Account, we seek to rationalize these findings using simple arguments based on considerations of orbital symmetry and the frontier molecular orbital theory.

The graphene conduction and valence bands (HOMO and LUMO) cross at the Dirac point, which defines the work function (W= 4.6 eV). Thus, the HOMO and LUMO form a degenerate pair of orbitals at this point in momentum space with the same ionization potential (IP) and electron affinity (EA). Based on the importance of the energies of the HOMO (-IP) and LUMO (-EA) in frontier molecular orbital (FMO) theory, graphene should be a reactive partner in Diels–Alder reactions due to the very high-lying HOMO and low-lying LUMO (energies of −4.6 eV). Inspection of the orbital symmetries of the degenerate pair of half-occupied band orbitals at the Dirac point confirms that with the appropriate orbital occupancies, both diene and dienophile reaction partners should undergo concerted Diels–Alder reactions with graphene that are allowed based on the Woodward–Hoffmann principles of orbital symmetry.

1. Introduction

The current focus on the various forms of graphene in the physics literature[1−3] has attracted the attention of the broader scientific community, and there is now worldwide interest in the chemical behavior of this very large polycyclic aromatic macromolecule. A number of interesting chemical transformations have been reported for the basal plane carbon atoms of graphene, and it is apparent that while it is thermodynamically very stable, graphene is able to participate in a variety of chemical reactions.[4,5]

In this Account, we discuss the facile reactivity of graphene in the Diels–Alder (DA) reaction and in particular its ability to function as both diene and dienophile under appropriate conditions,[6] and we show that the singular electronic structure of graphene is responsible for its unexpected chemical reactivity. In order to put the graphene results in context, we touch on the DA reactions of carbon nanotubes because their electronic structure is related to that of graphene, and we have included selected results from the literature on small organic molecules, where the results help to illuminate the discussion of graphene DA chemistry. The DA reaction is one of the most powerful and elegant reactions in organic chemistry, and we make no attempt to fully

Published on the Web 03/09/2012 www.pubs.acs.org/accounts
10.1021/ar200302g

SCHEME 1. Schematic Representation of the Diels–Alder Reaction between a Diene (1,3-Butadiene) and Dienophile (Ethylene), Illustrating the Diels–Alder Cycloaddition and Cycloreversion Reactions in Their Simplest Form[a]

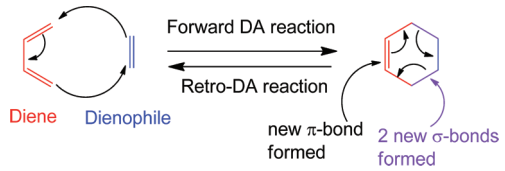

[a]The forward reaction leads to the formation of a six-membered ring via simultaneous creation of two new σ-bonds and one new π-bond and the loss of three π-bonds; alternatively, the process may be viewed as a change in hybridization in which four sp^2 carbon atoms become sp^3 hybridized.[9]

SCHEME 2. Canonical Resonance Structures of Graphene: Diene (**1**) and Dienophile (**2**)

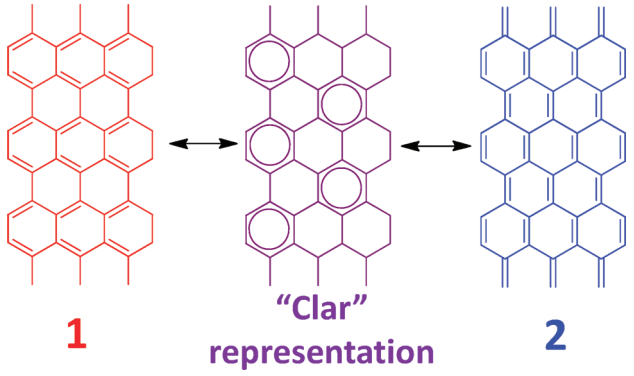

survey this important topic; fortunately there are excellent reviews available.[7]

Most molecules that participate in the Diels–Alder reaction do so as either diene or dienophile (Scheme 1), although there are exceptions to this generalization;[8] furthermore graphene is often considered to be highly aromatic and chemically stable, and aromatic molecules do not usually participate in thermal (ground-state) Diels–Alder reactions.

We attributed the dual reactivity of graphene in the Diels–Alder reaction to the absence of an energy gap (the valence and conduction bands touch at the Dirac point), which makes available a number of canonical structures (Scheme 2), thereby motivating the Diels–Alder reactivity of graphene and allowing it to function as both diene (**1**) and dienophile (**2**).[6]

In this Account, we examine this proposition from the standpoint of orbital symmetry[10] and frontier molecular orbital theory,[11] which together provide the key concepts for analyzing pericyclic reactions. As an introduction to this analysis, we first examine some simple, well-known DA reactions that have received detailed theoretical examination

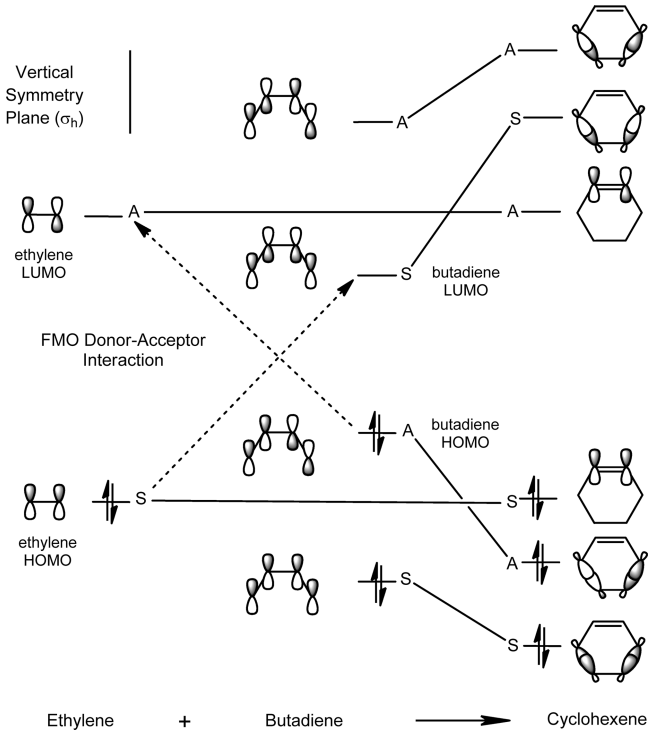

FIGURE 1. Diels–Alder orbital symmetry correlation diagram for the reaction of ethylene with butadiene,[10] together with frontier molecular orbital (FMO) interactions.[11] The orbitals are classified as either symmetric (S) or antisymmetirc (A) with respect to the vertical symmetry plane shown in the diagram.[10]

and that now may be used to instruct the basic theoretical concepts that come into play in assessing the DA reactivity of graphene.

2. The Diels–Alder Reaction Exemplified: Pericyclic Reaction between Ethylene and Butadiene

The orbital interactions in most pericyclic reactions may be analyzed from the standpoint of orbital symmetry and correlation diagrams between reactants and products or by a consideration of the frontier molecular orbitals of the reactants and their relative energies. In either case attention is focused on the highest occupied molecular orbitals (HOMOs) and lowest unoccupied molecular orbitals (LUMOs) of the reactants, and it is these orbitals that comprise the frontier molecular orbitals (FMOs); the two approaches are illustrated above in the classic reaction between butadiene (diene) and ethylene (dienophile) (Figure 1).[10,11]

From the standpoint of the correlation diagram it may be seen that the symmetries of the orbitals in reactant and product allow the smooth evolution of the electronic structure of the reaction complex along the reaction pathway.

While the energy gap between the reactant HOMOs and LUMOs narrows in the transition state, detailed calculations show that these orbitals do not cross along the reaction coordinate, and thus the orbital symmetries are rigorously maintained throughout the transformation between reactants and products.[11,12]

The frontier molecular orbital (FMO) theory considers only the reactant orbitals and analyzes the HOMO−LUMO interactions between reactants;[11,13] in principle, for the Diels−Alder reaction, this involves two pairs of HOMO−LUMO interactions, but because the FMO theory focuses on the energy separation between the interacting orbitals, it is often sufficient to consider a single HOMO−LUMO reactant interaction. The FMO analysis of the Diels−Alder reaction between butadiene and ethylene is shown on the left side of Figure 1; typically such an analysis is focused on the interaction between the butadiene (diene) HOMO and the ethylene (dienophile) LUMO, although reactions involving the converse situation (inverse electron demand) have been reported, and it is clear that both HOMO−LUMO interactions are operative to some degree in the Diels−Alder reaction. Implicit in the FMO treatment is the concept of charge transfer between reactants; that is, electron density is transferred from an occupied orbital (often the HOMO) of one reactant to a vacant orbital (often the LUMO) of the other reactant, and in this sense the FMO theory implies an orbital crossing, which at first sight seems to be at odds with the correlation diagram in Figure 1 and the results of detailed calculations.[12] The resolution of this difficulty is made clear if we consider the energy change (ΔE) that accompanies the interaction between the frontier orbitals from the standpoint of second-order perturbation theory

$$\Delta E = \frac{[H_{(\text{HOMO-ethylene}),(\text{LUMO-butadiene})}]^2}{\varepsilon_{\text{HOMO-ethylene}} - \varepsilon_{\text{LUMO-butadiene}}} + \frac{[H_{(\text{HOMO-butadiene}),(\text{LUMO-ethylene})}]^2}{\varepsilon_{\text{HOMO-butadiene}} - \varepsilon_{\text{LUMO-ethylene}}} \quad (1)$$

where the matrix elements in the numerators depend on the overlap and symmetry of the frontier orbitals of the two reactant molecules (exemplified here by ethylene and butadiene) and the denominators are the differences between the orbital energies of the frontier orbitals.

In fact, the FMO analysis may be recast in terms of a theory for the inclusion of configuration interaction in the wave function, which allows the admixture of excited states into the ground state of the reaction complex according to eq 1. In this way, the interactions between HOMOs and LUMOs in the reactants are understood to evolve along the reaction coordinate in the form of configurational mixing, and the intended correlations and charge transfer processes are therefore not rigorous in the same way as the orbitals involved in the construction of the correlation diagram. The FMO theory is particularly convenient in the present context because its application is confined to a consideration of the orbitals of the reactants and their energies [taken as the negative of the ionization potentials (−IP, HOMOs) and their electron affinities (−EA, LUMOs)]. As is clear from eq 1, FMO theory suggests that the appropriate HOMO−LUMO gap(s) (E_{H-L} = IP − EA), should provide an excellent inverse index of chemical reactivity,[11,13−15] and this is confirmed by an analysis of the rates of DA cycloadditions of dienes with cyanoalkenes in terms of the quantity $1/E_{H-L}$, where E_{H-L} = diene IP − cyanoalkene EA.[13] Thus the molecular HOMO−LUMO energy gap (E_{H-L}) may be regarded as an inverse measure of chemical reactivity; the larger the gap the lower is the reactivity. As shown below, it is the exceptionally low ionization potential (HOMO) and the exceptionally high electron affinity (LUMO) together with the absence of an energy gap that enables graphene to show dual nature of reactivity in Diels−Alder (DA) chemistry; that is, graphene can act as the diene or the dienophile and its reactivity is conveniently analyzed from just the same standpoint as the foregoing FMO treatment of the reaction between ethylene and butadiene and related molecules.

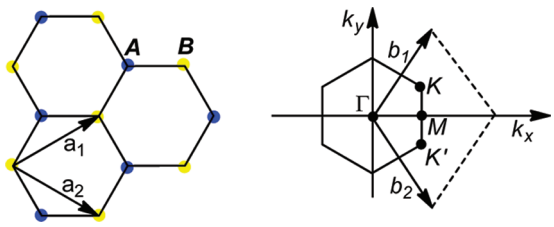

FIGURE 2. (a) Real space graphene lattice, showing the unit cell vectors and (b) Brillouin zone of graphene in momentum space.[3]

3. Electronic Structure of Graphene

We begin by introducing the electronic structure of graphene, which is now very well-known in the physics and chemistry literature, and the reader is directed to other works for details on this topic.[3] While all of the carbon atoms in graphene are equivalent in a chemical sense, there are two atoms in the unit cell, and thus in a crystallographic sense, the honeycomb structure of graphene is viewed as two interpenetrating triangular Bravais lattices, as depicted in Figure 2 because it is not possible to generate all of the lattice sites by simple translations of a single carbon atom.

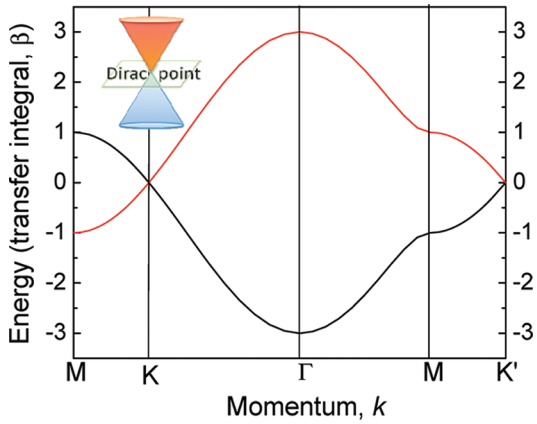

FIGURE 3. Graphene energy band dispersion in momentum space within simple tight-binding (HMO) theory; the resonance or transfer integral (β, **t**) has a value of about 3 eV.

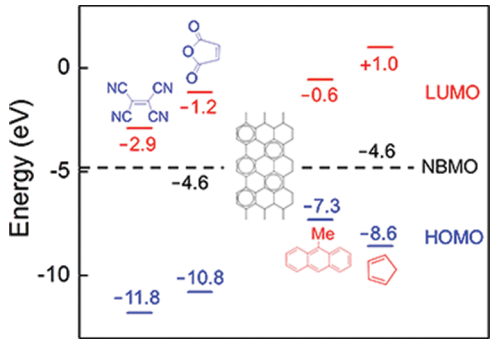

FIGURE 4. Orbital energies of selected dienes and dienophiles as obtained from ionization potentials (LUMO, −IP), electron affinities (HOMO, −EA), and the work function of graphene ($W = -4.6$ eV)[17] (adapted from Houk[15]). The neutrality point in graphene corresponds to the energy of the carbon-based nonbonding molecular orbital (NBMO).[18]

The Bravais lattices are traditionally labeled A and B, and the two different sets of carbon atoms are apparent in Figure 2; the primitive lattice vectors are given by $\mathbf{a}_1 = (3a/2)\mathbf{i} + (\sqrt{3}a/2)\mathbf{j}$ and $\mathbf{a}_2 = (3a/2)\mathbf{i} - (\sqrt{3}a/2)\mathbf{j}$ where a is the carbon−carbon bond length (1.421 Å) and **i** and **j** are the usual unit vectors along the x, y Cartesian axes; the reciprocal lattice vectors are given by $\mathbf{b}_1 = (2\pi/(3a))\mathbf{i} + (2\pi/(\sqrt{3}a))\mathbf{j}$ and $\mathbf{b}_2 = (2\pi/(3a))\mathbf{i} - (2\pi/(\sqrt{3}a))\mathbf{j}$. The first Brillouin zone may thus be obtained by taking perpendicular planes that bisect the vectors to the 6 nearest reciprocal lattice points. Thus the shape of the Brillouin zone is of the same form as the original six-membered rings of the honeycomb lattice in direct space, but rotated by 90°.

The band structure of graphene at the level of tight-binding theory with transfer integral **t** (resonance integral β, equivalent to the Huckel molecular orbital theory), was solved in 1947 by Wallace[16] (Figure 3). Two of the points at the corners of the Brillouin zone are distinct and are labeled by K and K′, whereas the other points are related to them by symmetry. As may be seen in Figure 3, the K points are particularly important because this is where the valence and conduction bands meet and cross, but it is important to note that the bands touch at a single point in **k** space, the Dirac Point, as a result of the crossing of the valence and conduction bands. For this reason, graphene is referred to as a zero band gap semiconductor, and the density of states at the Fermi level is zero (at the absolute zero of temperature).

Nevertheless the conductivity of graphene is always finite even when the chemical potential is at the Dirac point, and there are effectively no free carriers; furthermore the mobilities are extremely high and often limited by the underlying substrate. The transport properties of graphene are still the subject of intense research, and the high current densities that can be sustained in graphene together with the outstanding mobilities have motivated very strong interest in the use of graphene in the electronics industry. Graphene is now on the International Roadmap for Semiconductors, and in this regard the absence of a band gap in graphene is a serious problem because field-effect transistor devices fabricated from pristine graphene cannot be turned off; we return to this subject below because chemistry may well have a role to play in the band gap engineering of graphene.

We now turn to a consideration of the relevance of the band electronic structure of graphene to the question of its chemical reactivity with particular reference to the Diels−Alder reaction; as noted above, the orbital symmetry and FMO theories provide the most straightforward approach in the present context because we can carry out the analysis based on the orbital symmetries and energies of the parent graphene sheet. The analysis is based on the interaction between the HOMOs and LUMOs of reactants, which we take to be graphene with the prototype reaction partners ethylene and butadiene. Clearly with graphene when we consider the HOMO and LUMO, we confront a situation that is very different from a normal molecular system, because in graphene we have energy levels that cross at the Fermi level, the Dirac point (K). Thus according to the FMO theory, we should expect an extremely reactive macromolecule, and just as in the physics literature we focus on the Dirac point where there are two bands that provide the counterpart of the usual FMO donor−acceptor orbitals and constitute an exceptionally high-energy HOMO and an exceptionally low-energy LUMO. In fact the energies are the same at the Dirac point, and this determines the work function (W), which is approximately $W \approx 4.6$ eV, although it is dependent on the number of graphene layers;[17] for

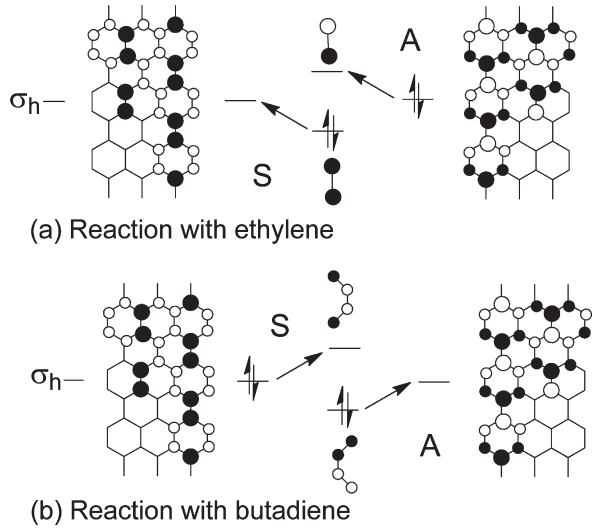

FIGURE 5. Orbital symmetry correlation diagram for the Diels–Alder reaction of ethylene and butadiene with graphene (FMOs taken from the band structure of graphene at the Dirac point, see text) where the signs of the lobes of the p orbitals above the plane are given by open and solid circles. The symmetry classification is based on the (σ_h) vertical symmetry plane; note that this symmetry plane is rotated by 90° from that used in Figure 1.

comparison we provide a selection of the HOMOs and LUMOs of typical Diels–Alder reactants in Figure 4.

In the study by Houk of the rates of DA cycloadditions of dienes with cyanoalkenes referred to above,[13] the highest rates were found in the reaction between 9,10-dimethylanthracene (DMA, IP = 7.1 eV) and tetracyanoethylene (TCNE, EA = 2.9 eV), for which E_{H-L} = IP − EA = 4.2 eV; whereas the DA reaction between graphene and TCNE has E_{H-L} = 1.7 eV and between DMA and graphene E_{H-L} = 2.5 eV.

Hence from a consideration of the orbital energies it is expected that graphene will be an extremely reactive DA partner, but in order to complete the analysis, it is now necessary to examine the symmetries of the graphene orbitals that might be involved and to delineate their role in DA chemistry based on their ability to function as donor or acceptor or both according to FMO theory. Thus we require knowledge of the FMO orbitals of graphene, that is, those orbitals that are most proximate to the Fermi level; in the case of graphene, we have orbitals that cross at the Dirac point, the K point in momentum space (**k**) (Figure 3).

The coefficients of the degenerate pair of orbitals at $\mathbf{k} = K = (2\pi/(3a), 2\pi/(3\sqrt{3}a))$ in momentum space, may be obtained by choice of the appropriate phase factor, and the real space representation of these orbitals has been given by Whangbo, Hoffmann, and Woodward.[19] The pair of orbitals at K is given above together with their symmetry with respect to the perpendicular symmetry plane, which is usually used for the orbital symmetry analysis of the DA reaction (Figures 1 and 5).[10]

The orbital correlation diagram (Figure 5) includes a number of unique features mainly related to the 2-fold degeneracy at the Dirac point; because of the degeneracy and the fact that this pair of orbitals is half-filled, there is a choice in the electronic configuration, and thus the electron pair may be accommodated in either the antisymmetric (A) graphene orbital (Figure 5a) or the symmetric (S) graphene orbital (Figure 5b), and this allows graphene to function as both donor and acceptor within FMO theory by matching the S or A orbital symmetries of its DA partner.[10,11] In the case of ethylene, the A graphene orbital donates electron density to ethylene, whereas the S orbital of graphene functions as an acceptor; the traditional picture would emphasize the former interaction.[13] Likewise, butadiene donates electron density into the empty A orbital of graphene and acts as acceptor from the S graphene orbital. Note that the orbital correlation diagram does not place any restrictions on the mode of pericyclic addition, and 1,2- and 1,4-cyclizations are allowed with both ethylene and butadiene; based on FMO theory,[11,13] the reactant atoms in graphene with the largest FMO coefficients should constitute the preferred sites of reaction. Thus according to this picture, graphene can function as diene or dienophile with equal ease; in practice graphene DA reaction preferences will depend on the orbital energies of the reacting partner, steric factors, and electron repulsion effects, which are not taken up in this Account.

4. Experimental Aspects of the Diels–Alder Reactions of Graphene

Graphene is available in various forms, and there is already strong evidence that the chemical and physical properties of the material are sensitive to the particular environment of the graphene sheet. Highly oriented pyrolytic graphite (HOPG) has been available for many years and is known to consist of oriented crystallites of graphene with a dimension of about 1 μm. Microcrystalline natural graphite (μG) is the most readily available commercial precursor for the generation of exfoliated graphenes;[1] single layer (SLG) and few layer graphenes (FLG) are typically obtained by exfoliation of natural graphite and studied as dispersions (XG_{sol}) or flakes (XG_{flake}), usually on a silicon dioxide substrate. Epitaxial graphene (EG) is typically grown on SiC by thermal desorption of Si above 1000 °C in vacuum or in an inert gas environment and is usually made available as rotationally disordered multilayer epitaxial graphene.[2,20] The interface layer has an energy gap and a rather complicated

SCHEME 3. Dual Nature of Reactivity of Graphene in Diels–Alder Chemistry[a]

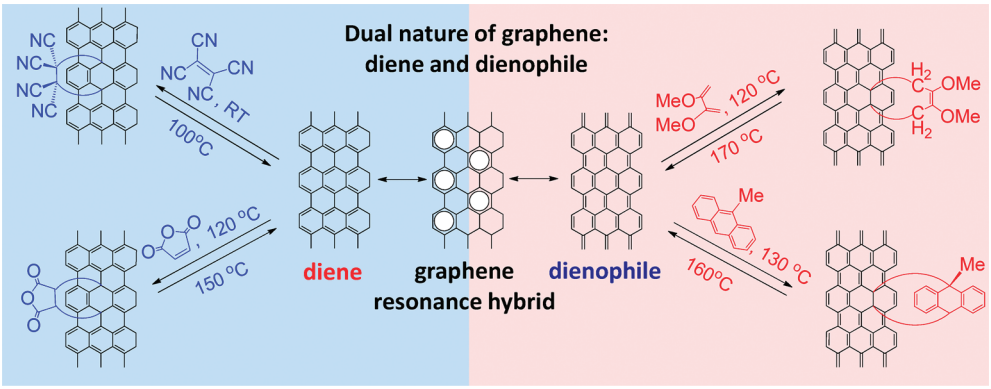

[a]Diene character of graphene (left), shown by its reactions with electron-deficient dienophiles (tetracyanoethylene and maleic anhydride), and dieneophile character of graphene (right), demonstrated by its reactivity towards electron-rich dienes (2,3-dimethoxy-1,3-butadiene and 9-methylanthracene).

electronic structure that includes the presence of covalent bonds between the graphene sheet and the underlying SiC, which induces variations in the carrier concentration (doping), the work function, and the graphene band structure near the Fermi level.[17,18] The enhanced reactivity of (multilayer) EG with respect to the Bernal-stacked graphite (μG and HOPG), discussed below, is of interest with respect to previous studies of the reactivity of the various forms of graphene;[21−23] apart from the differences discussed above, an obvious distinction is the splitting that occurs at the K point in graphene as a result of the interlayer interaction[24] (see Figure 3). At the level of simple tight binding theory (Figure 3), allowance for additional transfer integrals to describe the various interactions in the 3-D graphite lattice leads to a bandwidth of ~1.5 eV at the K points, and the material becomes a semimetal with a band overlap of ~0.1 eV.[24]

An important distinction between the macroscopic HOPG and EG samples and the various forms of XG relates to specimen sizes and the availability of a well-defined surface. The conversion of sp^2 to sp^3 carbon atoms due to chemical reaction leads to distinct changes in the Raman spectra of graphene,[22,25] and the presence of a D-band in the Raman spectrum of functionalized graphene is routinely used as evidence for covalent bond formation.[4,6,22,25−28]

Our current experimental findings are summarized in Scheme 3, and it is apparent that graphene reversibly undergoes DA reactions with various reaction partners and is able to function as diene or dienophile as suggested by the foregoing analysis (Figures 4 and 5).

4.1. Graphene as Diene. Graphene was found to be very reactive toward tetracyanoethylene (TCNE), and the reactions proceed at room temperature[6] (in agreement with the very low value of E_{H-L} = 1.7 eV calculated for this reaction, above), whereas functionalization with maleic anhydride (MA) required a reaction temperature of about 120 °C, presumably as a result of the higher value of E_{H-L} = 3.4 eV calculated for this reaction. There is already strong evidence for doping reaction channels (electron-transfer processes), which compete with covalent functionalization reactions in graphene chemistry,[18,29] and we observed the occurrence of p-type doping (oxidation) by the highly electron-deficient reagent tetracyanoethylene (TCNE, electron affinity =2.88 eV)[13] in preference to the simple Diels–Alder reaction.

4.2. Graphene as Dienophile. The optimum temperature for the Diels–Alder reactions with DMBD was found to depend on the nature of the graphitic material as follows: HOPG (130 °C), μG (120 °C), XG_{sol} (130 °C), and EG (50 °C).[6] The reaction can be reversed in all cases at about 170 °C, switching the functionalized graphene back to the pristine material. The reaction of microcrystalline graphite (μG) with the electron-rich diene 2,3-dimethoxy-1,3-butadiene (DMBD) was found to be a particularly effective route for producing stable colloidal dispersions of single-layer functionalized graphene flakes from graphite, as evidenced by the sharp 2D peak (located at ~2684 cm^{-1}, with $I_{2D}/I_G = 0.73$) in the Raman spectra of the resulting DMBD–μG materials (Figure 6b).[6] There is considerable interest in using such functionalization schemes to produce bulk quantities of solution redispersible graphene materials that do not readily aggregate in solution,[30−32] and the covalent Diels–Alder functionalization approach is a viable option in this regard, particularly because of the clean reversibility of the reaction.

The electronic structure of the graphene surface after DA chemistry is of great interest from the standpoint of the application of organic chemical process lithography to the band gap engineering of graphene devices.[18] The transport

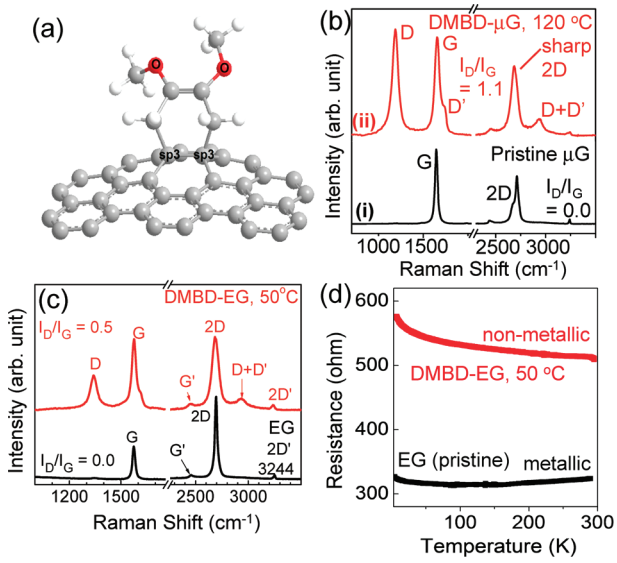

FIGURE 6. (a) Three-dimensional structure of the Diels–Alder adduct of graphene and 2,3-dimethoxy-1,3-butadiene (DMBD), showing the creation of a pair of sp^3 carbon centers in the graphene lattice and the generation of a slightly nonplanar structure. (b) Raman spectra (λ_{ex} = 532 nm) of pristine microcrystalline graphite (μG) and its Diels–Alder adduct, DMBD–μG, obtained at 120 °C. (c) Raman spectra (λ_{ex} = 532 nm) of pristine epitaxial graphene (EG) and its Diels–Alder adduct, DMBD–EG, obtained at 50 °C. (d) Temperature-dependent resistance of EG wafer (before reaction) and DMBD–EG (after reaction); functionalization of EG with DMBD leads to a 60% increase in room temperature resistance, and the DMBD–EG shows nonmetallic behavior over the full temperature range.

properties of DMBD–EG (Figure 6d) show a change in the character of the measured electrical resistance of the graphene wafer after covalent Diels–Alder functionalization, indicating that chemistry on the top layer of epitaxial graphene (EG) is quite efficient in modifying the electronic structure of the graphene sheet.

A particularly direct probe of the electronic structure of the functionalized graphene surface is afforded by scanning tunneling microscopy (STM), which can also give the surface coverage of the functional groups and their periodicities over the whole graphene wafer; however, this technique typically requires ultrahigh vacuum and cryogenic temperatures.[18,33,34]

Both theoretical calculations and experimental data have shown that single atom sp^3 functionalization sites that result from a radical addition process, in both graphite and graphene, generate 3-fold symmetric patterns in the local density of states (LDOS) as a result of presence of the unpaired spin, which is localized in the vicinity of the point of addition.[18,35–38] These patterns can be enhanced by two-dimensional fast Fourier transform (2D-FFT) filtering of STM images acquired under ambient conditions, and it has been shown that positive and negative spin densities become

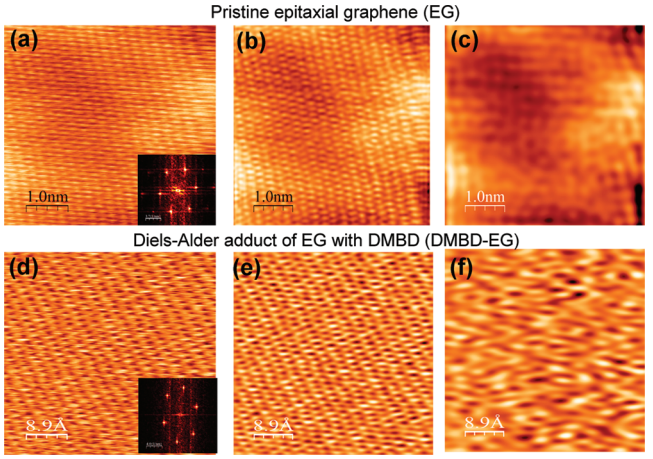

FIGURE 7. STM current images of pristine EG (a,b,c) and 2,3-dimethoxy-1,3-butadiene functionalized epitaxial graphene, DMBD–EG (d,e,f) under ambient conditions. (a) Pristine EG, V_{bias} = +5.1 mV, I_t = 4.3 nA; 2D-FFT spectrum of the STM image is shown in the inset. (b) STM image of EG after subtracting noise. (c) 2D-FFT filtered STM image of EG. (d) DMBD–EG, V_{bias} = +5 mV, I_t = 3 nA; 2D-FFT spectrum of the STM image is shown in the inset. (e) STM image of DMBD-EG after subtracting noise. (f) 2D-FFT filtered STM image of DMBD–EG.

localized at the **A** and **B** sublattices, in a 3-fold symmetric superlattice.[36] The Diels–Alder cycloaddition chemistry is expected to occur by the pairwise formation of 1,4- or 1,2-sp^3 carbon centers in the regular honeycomb lattice of sp^2 carbon atoms, and thus antiferromagnetic (diamagnetic) products are expected,[39] because this pattern of chemistry guarantees the balanced functionalization of the **A** and **B** graphene sublattices. Hence the electronic structure of the Diels–Alder functionalized graphene lattice will be completely different from that formed in the atom-by-atom reactions of graphene with nitrophenyl radicals or hydrogen atoms.[18,34–38]

The STM images of defect-free, pristine 1–3 layer EG and DMBD–EG are compared in Figure 7; the STM images are collected using a Digital Instruments Nanoscope IIIa multimode scanning probe microscope (Pt/Ir tips) under ambient conditions. The 2D FFT spectrum of the STM image of EG consists of six outer bright spots from the graphene superlattice and six spots corresponding to the graphene lattice in the center, which appear as the large bright spot at the center in the insets of Figure 7a,d. The higher order spots are filtered in the FFT spectrum (Figure 7b,e), which improves the image by removing the noise, whereas in Figure 7c,f, the graphene lattice is also filtered by removing everything inside the largest circle circumscribed by the hexagon of the superlattice points, yielding an image that reflects the modified LDOS.[18] The 2D-FFT filtered LDOS given in Figure 7f shows scattering and interference patterns over the entire image, and it is clear from Figure 7c,f that the DA reaction with

DMBD leads to a striking reconstruction of the epitaxial graphene electronic structure.

5. Diels–Alder Reactivity of Carbon Nanotubes

The electronic structure of singe-walled carbon nanotubes (SWNTs) is more complicated than that of graphene because the cylindrical structure allows the possibility of a variety of diameters and chiralities. The variation in diameter leads to structures with different strain, and this is reflected in the pyramidalization angles, which are much smaller than those in the fullerenes, and the π-orbital misalignment angles, which are sometimes greater than those in the fullerenes.[40,41] However, it is the variation in chirality that affects the energy spectrum (Figure 8), and metallic and semiconducting SWNTs are known to occur in a 1:2 ratio in the usual preparations; the small band gap in the SWNTs (~1 eV for the semiconductors and zero in the case of the metals) suggests that Diels–Alder chemistry may be favorable.

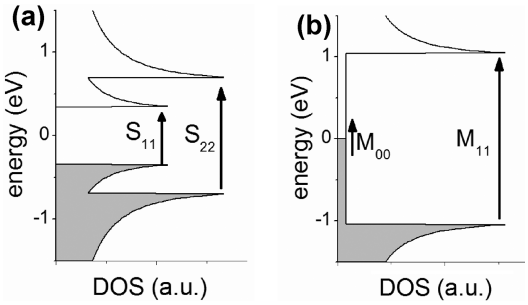

FIGURE 8. Density of states (DOS) as a function of energy for single-walled carbon nanotubes (SWNTs), together with allowed interband transitions: (a) semiconductors, S_{11} and S_{22}, and (b) metals, M_{00} and M_{11}.

The Diels–Alder reaction is known to occur with carbon nanotubes, and it has been found experimentally that *o*-quinodimethane reacts with soluble SWNTs,[42] while fluorinated SWNTs undergo cycloaddition reactions with dienes.[43] It was shown that pristine SWNTs could be activated by interaction with $-Cr(CO)_3$[44–46] and the application of high pressure (Scheme 4a).[44]

The Diels–Alder reaction chemistry of pristine HiPCO SWNTs toward fluorinated olefins was proposed to proceed by a [2 + 2] cycloaddition;[47] this chemistry was able to eliminate or completely transform metallic carbon nanotubes into semiconductors, thereby resulting in field effect transistors with reasonable on–off ratios (1:100 000) while retaining high mobilities (~100 $cm^2\ V^{-1}\ s^{-1}$) in these devices.

Recently, the Diels–Alder chemistry between single-walled carbon nanotubes (SWNTs) and an electron-rich diene (1-aminoanthracene) was suggested to be selective toward semiconducting carbon nanotubes (Scheme 4b), suggesting the initial applications of this chemistry in the

SCHEME 4. Diels–Alder Reactivity of Pristine Single-Walled Carbon Nanotubes (SWNTs)[a]

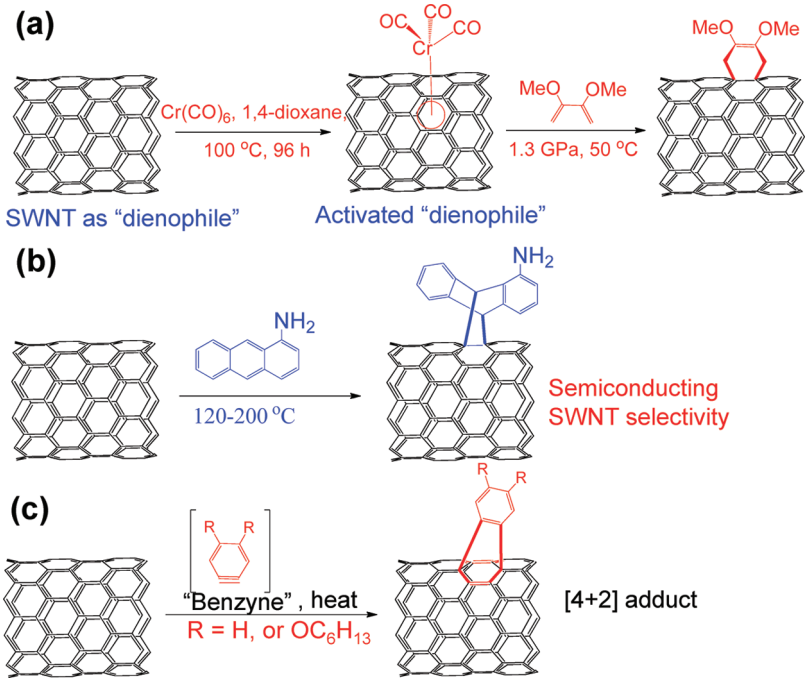

[a](a) Activation of SWNTs using chromium hexacarbonyl and subsequent reaction with an electron-rich diene, 2,3-dimethoxy-1,3-butadiene.[44] (b) Preferential reactivity of 1-aminoanthracene towards semiconducting-SWNTs.[48] (c) Benzyne addition reactions of SWNTs.[49]

separation of metallic (M) and semiconducting (SC) single-walled carbon nanotubes.[48] The addition of benzyne to carbon nanotubes (Scheme 4c) has been reported to occur preferentially with larger diameter SWNTs as a result of the more favorable electronic structure (lower band gap).[49] Diels–Alder chemistry has also been suggested to play a role in the polymerization of small molecules to produce single-walled carbon nanotube by rational synthesis.[50]

6. Conclusions and Outlook

The selective chemical modification and patterning of graphene wafers with atomic precision would provide the post-CMOS manufacturing technology necessary for carbon-based lithography,[18] and in this regard the Diels–Alder chemistry discussed herein offers an attractive avenue for the pairwise, reversible formation of sp^3 carbon centers in the graphene lattice. Our analysis provides a basic understanding of the facile Diels–Alder processes exhibited by graphene from the organic chemistry standpoint of orbital symmetries and energies, but leaves many unanswered questions such as the exact nature of the addition products, their density and the electronic structure of the functionalized graphene lattice – that is, the chemistry beyond the Dirac point.

The authors acknowledge financial support from DOD/DMEA under contract H94003-10-2-1003 and NSF-MRSEC through contract DMR-0820382.

Note Added after ASAP Publication. This manuscript was published ASAP on March 9, 2012 with missing data in the caption of Figure 4. The corrected version was reposted on March 14, 2012.

BIOGRAPHICAL INFORMATION

Santanu Sarkar obtained his M.Sc. degree in Chemistry from Indian Institute of Technology, Madras. As visiting research scholar, Santanu worked for three years at the University of Nebraska, Lincoln, on synthesis and biological applications of organic nitroxide and aminyl radicals for spin-labeling applications with Professor Andrzej Rajca. He is currently a Ph.D. candidate at University of California, Riverside, under the supervision of Professor Robert C. Haddon with a focus on covalent chemical functionalization and spectroscopy of epitaxial and exfoliated graphene devices for applications in graphene electronics.

Elena Bekyarova obtained her Ph.D. degree in Chemistry from the Bulgarian Academy of Sciences. She is currently an Associate Researcher at the University of California, Riverside.

Robert C. Haddon is Distinguished Professor and Director of the Center for Nanoscale Science and Engineering at the University of California, Riverside. He shared the 2008 APS James P McGroddy Prize for New Materials and is the recipient of the 2010 ECS Richard E Smalley Research Award. http://www.eng.ucr.edu/faculty/chemenv/haddon.html.

FOOTNOTES

The authors declare no competing financial interest.

REFERENCES

1 Novoselov, K. S.; Geim, A. K.; Morozov, S. V.; Jiang, D.; Zhang, Y.; Dubonos, S. V.; Grigorieva, I. V.; Firsov, A. A. Electric Field Effect in Atomically Thin Carbon Films. *Science* **2004**, *306*, 666–669.

2 Berger, C.; Song, Z.; Li, T.; Li, X.; Ogbazghi, A. Y.; Feng, R.; Dai, Z.; Marchenkov, A. N.; Conrad, E. H.; First, P. N.; de Heer, W. A. Ultrathin Epitaxial Graphite: 2D Electron Gas Properties and a Route toward Graphene-Based Nanoelectronics. *J. Phys. Chem. B* **2004**, *108*, 19912–19916.

3 Castro Neto, A. H.; Guinea, F.; Peres, N. M. R.; Novoselov, K. S.; Geim, A. K. The Electronic Properties of Graphene. *Rev. Mod. Phys.* **2009**, *81*, 109–162.

4 Loh, K. P.; Bao, Q. L.; Ang, P. K.; Yang, J. X. The Chemistry of Graphene. *J. Mater. Chem.* **2010**, *20*, 2277–2289.

5 Bekyarova, E.; Sarkar, S.; Niyogi, S.; Itkis, M. E.; Haddon, R. C. Advances in the Chemical Modification of Epitaxial Graphene. *J. Phys. D: Appl. Phys.* **2012**, *in press Special issue: Epitaxial Graphene.*

6 Sarkar, S.; Bekyarova, E.; Niyogi, S.; Haddon, R. C. Diels–Alder Chemistry of Graphite and Graphene: Graphene as Diene and Dienophile. *J. Am. Chem. Soc.* **2011**, *133*, 3324–3327.

7 Nicolaou, K. C.; Snyder, S. A.; Montagnon, T.; Vassilikogiannakis, G. The Diels–Alder Reaction in Total Synthesis. *Angew. Chem., Int. Ed.* **2002**, *41*, 1668–1698.

8 Munirasu, S.; Albuerne, J.; Boschetti-de-Fierro, A.; Abetz, V. Functionalization of Carbon Materials Using the Diels–Alder Reaction. *Macromol. Rapid Commun.* **2010**, *31*, 574–579.

9 Haddon, R. C.; Chow, S.-Y. Hybridization as a Metric for the Reaction Coordinate of Chemical Reactions. *J. Am. Chem. Soc.* **1998**, *120*, 10494–10496.

10 Woodward, R. B.; Hoffmann, R. *The Conservation of Orbital Symmetry*; VCH: Weinheim, Germany, 1970.

11 Fukui, K. Theory of Orientation and Stereoselection. *Top. Curr. Chem.* **1970**, *15*, 1–85.

12 Townshend, R. E.; Ramunni, G.; Segal, G.; Hehre, W. J.; Salem, L. Organic Transitions States. V. The Diels–Alder Reaction. *J. Am. Chem. Soc.* **1976**, *98*, 2190–2198.

13 Houk, K. N. The Frontier Molecular Orbital Theory of Cycloaddition Reactions. *Acc. Chem. Res.* **1975**, *8*, 361–369.

14 Fukui, K. Recognition of Stereochemical Paths by Orbital Interaction. *Acc. Chem. Res.* **1971**, *4*, 57–64.

15 Houk, K. N.; Munchausen, L. L. Ionization Potentials, Electron Affinities, and Reactivities of Cyanoalkenes and Related Electron-Deficient Alkenes. A Frontier Molecular Orbital Treatment of Cyanoalkene Reactivities in Cycloadditon, Electrophilic, Nucleophilic, and Radical Reactions. *J. Am. Chem. Soc.* **1976**, *98*, 937–946.

16 Wallace, P. R. The Band Theory of Graphite. *Phys. Rev.* **1947**, *71*, 622–634.

17 Mathieu, C.; Barrett, N.; Rault, J.; Mi, Y. Y.; Zhang, B.; de Heer, W. A.; Berger, C.; Conrad, E. H.; Renault, O. Microscopic Correlation between Chemical and Electronic States in Epitaxial Graphene on SiC(0001). *Phys. Rev. B* **2011**, *83*, No. 235436.

18 Niyogi, S.; Bekyarova, E.; Hong, J.; Khizroev, S.; Berger, C.; de Heer, W. A.; Haddon, R. C. Covalent Chemistry for Graphene Electronics. *J. Phys. Chem. Lett.* **2011**, *2*, 2487–2498.

19 Whangbo, M.-H.; Hoffmann, R.; Woodward, R. B. Conjugated One and Two Dimensional Polymers. *Proc. R. Soc. London A* **1979**, *366*, 23–46.

20 de Heer, W. A.; Berger, C.; Wu, X.; Sprinkle, M.; Hu, Y.; Ruan, M.; Stroscio, J.; First, P. N.; Haddon, R. C.; Piot, B.; Faugeras, C.; Potemski, M.; Moon, J.-S. Epitaxial Graphene Electronic Structure and Transport. *J. Phys. D: Appl. Phys.* **2010**, *43*, No. 374007.

21 Liu, H.; Ryu, S.; Chen, Z.; Steigerwald, M. L.; Nuckolls, C.; Brus, L. E. Photochemical Reactivity of Graphene. *J. Am. Chem. Soc.* **2009**, *131*, 17099–17101.

22 Koehler, F. M.; Jacobsen, A.; Ensslin, K.; Stampfer, C.; Stark, W. J. Selective Chemical Modification of Graphene Surfaces: Distinction between Single- and Bilayer Graphene. *Small* **2010**, *6*, 1125–1130.

23 Sharma, R.; Baik, J. H.; Perera, C. J.; Strano, M. S. Anomalously Large Reactivity of Single Graphene Layers and Edges toward Electron Transfer Chemistries. *Nano Lett.* **2010**, *10*, 398–405.

24 Dresselhaus, M. S.; Dresselhaus, G. Intercalation Compounds of Graphite. *Adv. Phys.* **2002**, *51*, 1–186.

25 Niyogi, S.; Bekyarova, E.; Itkis, M. E.; Zhang, H.; Shepperd, K.; Hick, J.; Sprinkle, M.; Berger, C.; Lau, C. N.; de Heer, W. A.; Conrad, E. H.; Haddon, R. C. Spectroscopy of Covalently Functionalized Graphene. *Nano Lett.* **2010**, *10*, 4061–4066.

26 Ryu, S.; Han, M. Y.; Maultzsch, J.; Heinz, T. F.; Kim, P.; Steigerwald, M.; Brus, L. E. Reversible Basal Plane Hydrogenation of Graphene. *Nano Lett.* **2008**, *8*, 4597–4602.

27 Elias, D. C.; Nair, R. R.; Mohiuddin, T. M. G.; Morozov, S. V. B. P.; Halsall, M. P.; Ferrari, A. C.; Boukhvalov, D. W.; Katsnelson, M. I.; Geim, A. K.; Novoselov, K. S. Control of Graphene's Properties by Reversible Hydrogenation: Evidence for Graphane. *Science* **2009**, *323*, 610–613.

28 Luo, Z.; Yu, T.; Kim, K.-J.; Ni, Z.; You, Y.; Lim, S.; Shen, Z.; Wang, S.; Lin, J. Thickness-Dependent Reversible Hydrogenation of Graphene Layers. *ACS Nano* **2009**, *3*, 1781–1788.

29 Farmer, D. B.; Golizadeh-Mojarad, R.; Perebeinos, V.; Lin, Y.-M.; Tulevski, G. S.; Tsang, J. C.; Avouris, P. Chemical Doping and Electron-Hole Conduction Asymmetry in Graphene Devices. *Nano Lett.* **2009**, *9*, 388–392.

30 Swager, T. M. Functional Graphene: Top-Down Chemistry of the π-Surface. *ACS Macro Lett.* **2012**, *1*, 3–5.

31 Zhong, X.; Jin, J.; Li, S.; Niu, Z.; Hu, W.; Li, R.; Ma, J. Aryne Cycloaddition: Highly Efficient Chemical Modification of Graphene. *Chem. Commun.* **2010**, *46*, 7340–7342.

32 Englert, J. M.; Dotzer, C.; Yang, G. A.; Schmid, M.; Papp, C.; Gottfried, J. M.; Steinruck, H. P.; Spiecker, E.; Hauke, F.; Hirsch, A. Covalent Bulk Functionalization of Graphene. *Nat. Chem.* **2011**, *3*, 279–286.

33 Hossain, M. Z.; Walsh, M.; Hersam, M. C. Scanning Tunneling Microscopy, Spectroscopy, and Nanolithography of Epitaxial Graphene Chemically Modified with Aryl Moieties. *J. Am. Chem. Soc.* **2010**, *132*, 15399–15403.

34 Balog, R.; Jorgensen, B.; Wells, J.; Laegsgaard, E.; Hofmann, P.; Besenbacher, F.; Hornekaer, L. Atomic Hydrogen Adsorbate Structures on Graphene. *J. Am. Chem. Soc.* **2009**, *131*, 8744–8745.

35 Yazyev, O. V. Emergence of Magnetism in Graphene Materials and Nanostructures. *Rep. Prog. Phys.* **2010**, *73*, No. 056501.

36 Kelly, K. F.; Halas, N. J. Determination of α and β Site Defects on Graphite Using C_{60}-Adsorbed STM Tips. *Surf. Sci.* **1998**, *416*, L1085–L1089.

37 Ruffieux, P.; Groning, O.; Schwaller, P.; Schlapbach, L.; Groning, P. Hydrogen Atoms Cause Long-Range Electronic Effects on Graphite. *Phys. Rev. Lett.* **2000**, *84*, 4910–4913.

38 Ruffieux, P.; Melle-Franco, M.; Groning, O.; Bielmann, M.; Zerbetto, F.; Groning, P. Charge-Density Oscillation on Graphite Induced by the Interference of Electron Waves. *Phys. Rev. B* **2005**, *71*, No. 153403.

39 Hong, J.; Niyogi, S.; Bekyarova, E.; Itkis, M. E.; Palanisamy, R.; Amos, N.; Litvinov, D.; Berger, C.; de Heer, W. A.; Khizroev, S.; Haddon, R. C. Effect of Nitrophenyl Functionalization on the Magnetic Properties of Epitaxial Graphene. *Small* **2011**, *7*, 1175–1180.

40 Haddon, R. C. Chemistry of the Fullerenes: The Manifestation of Strain in a Class of Continuous Aromatic Molecules. *Science* **1993**, *261*, 1545–1550.

41 Niyogi, S.; Hamon, M. A.; Hu, H.; Zhao, B.; Bhowmik, P.; Sen, R.; Itkis, M. E.; Haddon, R. C. Chemistry of Single-Walled Carbon Nanotubes. *Acc. Chem. Res.* **2002**, *35*, 1105–1113.

42 Delgado, J. L.; de la Cruz, P.; Langa, F.; Urbina, A.; Casado, J.; Navarrete, J. T. L. Microwave Assisted Sidewall Functionalization of Single-wall Carbon Nanotubes by Diels–Alder Cycloaddition. *Chem. Commun.* **2004**, *15*, 1734–1735.

43 Zhang, L.; Yang, J. Z.; Edwards, C. L.; Alemany, L. B.; Khabashesku, V. N.; Barron, A. R. Diels–Alder Addition to Fluorinated Single Walled Carbon Nanotubes. *Chem. Commun.* **2005**, 3265–3267.

44 Menard-Moyon, C.; Dumas, F.; Doris, E.; Mioskowski, C. Functionalization of Single-Wall Carbon Nanotubes by Tandem High-Pressure/$Cr(CO)_6$ Activation of Diels–Alder Cycloaddition. *J. Am. Chem. Soc.* **2006**, *128*, 14764–14765.

45 Nunzi, F.; Sgamellotti, A.; De Angelis, F. $Cr(CO)_3$-Activated Diels-Alder Reaction on Single–Wall Carbon Nanotubes: A DFT Investigation. *Chem.—Eur. J.* **2009**, *15*, 4182–4189.

46 Sarkar, S.; Niyogi, S.; Bekyarova, E.; Haddon, R. C. Organometallic Chemistry of Extended Periodic π-Electron Systems: Hexahapto-Chromium Complexes of Graphene and Single-Walled Carbon Nanotubes. *Chem. Sci.* **2011**, *2*, 1326–1333.

47 Kanungo, M.; Lu, H.; Malliaras, G. G.; Blanchet, G. B. Suppression of Metallic Conductivity of Single-Walled Carbon Nanotubes by Cycloaddition Reactions. *Science* **2009**, *323*, 234–237.

48 Sun, J. T.; Zhao, L. Y.; Hong, C. Y.; Pan, C. Y. Selective Diels–Alder Cycloaddition on Semiconducting Single-Walled Carbon Nanotubes for Potential Separation Application. *Chem. Commun.* **2011**, *47*, 10704–10706.

49 Criado, A.; Gomez-Escalonilla, M. J.; Fierro, J. L. G.; Urbina, A.; Pena, D.; Guitian, E.; Langa, F. Cycloaddition of Benzyne to SWNT: Towards CNT-Based Paddle Wheels. *Chem. Commun.* **2010**, *46*, 1272–1274.

50 Fort, E. H.; Donovan, P. M.; Scott, L. T. Diels–Alder Reactivity of Polycyclic Aromatic Hydrocarbon Bay Regions: Implications for Metal-Free Growth of Single-Chirality Carbon Nanotubes. *J. Am. Chem. Soc.* **2009**, *131*, 16006–16007.